論文

Duration time detection of Forest Fire by Advanced HIMAWARI-8 Imager (AHI) for Indonesian peat fires in 2015.

2105年インドネシア泥炭地での森林火災の Advanced HIMAWARI-8 Imager（AHI）による継続時間の検出

Etsuko NAKAZONO, Wataru TAKEUCHI* and Masao MORIYAMA***
中園　悦子・竹内　　渉・森山　雅雄

Abstract : We investigated the feasibility of using the Himawari-8, a Japanese meteorological geostationary satellite with high temporal resolution (receiving data at 10-minute intervals), to measure the time from fire outbreak to extinction. We selected the study area in Central Kalimantan, in Indonesia, containing peatland. We first investigated which band of Advanced Himawari Imager (AHI) is more sensitive for detecting fire areas and which band is suitable for tracking time-series change of fire area. Therefore, we first used the Landsat 8 data of 2015/10/22 for visual interpretation of the fire area and then selected pixels corresponding to the fire area from the AHI data acquired at about the same time as the Landsat 8 data. We found that band 7 of the AHI is the most suitable for detecting fire area even if the ratio of fire area in one pixel is low, and we assumed that not only high values of band 7 but also the short-term fluctuations are characteristics of fires. To establish this assumption, we separated the value of band 7 into 2 components, mean value and short-term fluctuations, μtm, and Dtm, respectively. Then, we applied these two indices to the data for September 2015 and confirmed how fire occurrence and extinguishment were captured by these two indices.

Keywords : keyword 1 high temporal resolution ; keyword 2 mid-infrared ; keyword 3 short-term fluctuations

1．Introduction

In recent years, large-scale fires have been frequent. Liu et al. (2013) showed that fire potential is expected to increase in many regions across the continental United States, mainly caused by future warming trends. Jolly et al. (2015) showed a 108.1% increase in global burnable area, affected by a global increase in the length of fire weather seasons during the second half of the study period. Additionally, the IPCC (2014) has predicted that forest fires will become more frequent with global warming. Therefore, the early detection of forest fires has become a more important problem in recent years. And satellite data is one of the useful tools to detect fires in a wide range.

In general, for early detection of forest fires, it is necessary to use satellite data with at least medium spatial resolution (～1 km) and high temporal resolution (Schroeder et al. (2008), Fuchs et al. (2015)). For this purpose, several satellites from the 1980s have been used to detect forest fires. Many papers have been published about this type of fire detection, using sun-synchronous polar-orbiting satellites such as NOAA AVHRR (e.g. Cahoon et al. (1994), Rauste et al. (1997), Boles and Verbyla (1999), Giglio et al. (1999)), MODIS (e.g. Seielstad et al. (2000), Giglio et al. (2003), Morisette et al. (2005), Hawbaker et al. (2008), Freeborn et al. (2014), Giglio et al. (2016)), and Landsat (Bohme et al. (2015), Schroeder et al. (2016)). However, the temporal resolution of these sun-synchronous polar-orbiting satellites is low to find out forest fires early and observe the expansion of their damage continuously.

* Institute of Industrial Science, the University of Tokyo
**Nagasaki University

Geostationary satellites are also being used for fire detection. The range of the geostationary satellite observation space is limited and the spatial resolution is low. Then the fire detection capability of geostationary satellites tends to be lower than that of the sun-synchronous polar-orbiting satellites (Schroeder et al. (2010)). However, the temporal resolutions of geostationary satellites are very high compared with the sun-synchronous polar-orbiting satellite and it is possible to monitor the fire in succession (Calle et al. (2006), Xu et al. (2010)).

Temporally continuous fire observation is important in several ways. To measure the recovery of the vegetation in a burnt area, it is important to analyze the details of the actual fire. An interaction exists between the forest fire regime and forest landscape structure (Bonan and Shugart (1989), Lecomte et al. (2006)). Many papers have developed spatial models that demonstrate the interactions between forest fires and forest landscape (Antonovsky et al. (1989), Li et al. (1995)). Keane et al. (2004) classified 45 landscape fire succession models according to fire ignition, fire spread, fire effects, and vegetation succession, and some papers have been published that compare these models (Cary et al., 2006, Yang et al. (2008)). If it is possible continuous observation of the fire by geostationary satellites with sufficiently short observation time intervals, we can observe the forest fire, which is similar to real-time observation and is possible to observe the speed and direction of fire spread, in particular, the fire characteristics listed by Kerne.

And it is also important to measure the period from fire occurrence to extinguishment for determining the amount of burnt biomass. Wooster et al (2005) showed that the relationship between FRP (Fire Radiative Power, measure of the rate of radiant heat output from a fire) calculated from MIR (Mid-Infrared) band of SEVIRI, the sensor in Meteosat8 and the burned fuel mass is linear and from the fire period and the fuel mass per unit time that estimation is possible for burned-out biomass.

To monitor the fire from occurrence to extinguishment, we selected Himawari-8. Himawari-8 is a Japanese weather stationary satellite that was launched in October 2014 and became fully operational in July 2015 (Bessho et al. (2016)). The satellite has a new payload called the Advanced Himawari Imager (AHI), a sixteen-channel multispectral imager with high spatial resolutions of 0.5 to 2 km, compared to other geostationary satellites. From the AHI, data are received every 10 minutes, meaning the temporal resolution is high enough for the early detection of forest fires. Then some papers have already been published about not only to detect the forest fires in coverage of AHI (e.g. Fatkhuroyan et al. (2017) in Indonesia, Na et al. (2018) in China-Mongolia Border Regions, Liu et al. (2018) in China-Russia Border area, Jang et al. (2019) in South Korea) but also to retrieve the FRP by using AHI data (Xu et al., 2019).

In this paper, we aimed to follow from occurrence to extinguishment of fire, measure the period of fire in the peatland. Fires in peatland area emit a large amount of carbon, and the impact of peat fires affect not only Indonesia but also the surrounding countries, which is one of the serious environmental problems (Wiggins et al. (2018)). Carbon was released from not only the tree and vegetation but also peat combustion. Also, Smoldering is a major combustion process in peat fires, releasing large amounts of carbon and smoke into the atmosphere (Huang and Rain, 2019). Page et al. (2002) estimated that between 0.81 and 2.57 Gt of carbon were released to the atmosphere in 1997, an El Nino year, as a result of burning peat and vegetation in Indonesia. Since peatland fires often take a long time to extinguish and the scale of the fire is large, geostationary satellites with low spatial resolution are expected to track the fire's temporal changes. We examined whether changes in the value of AHI could track the time-series change from fire occurrence to extinguishment. To do so, we first need to identify which band of the AHI is suitable for tracking the time-series change of the fire. Then, we compared the values of the AHI pixels at the fire

location with the values of the non-fire pixels to see which indices were suitable for observing the time-series change of the fire. Next, we used fire data from different periods at the same location to see if the AHI indices could track the time-series change of the fire area.

2. Method

2.1 Selecting the Study area and Data

We selected a study area within Indonesia because many large-scale forest fires occurred from September to October 2015. According to the peatland map of Badan Restorasi Gambut (BRG, Peatland Restoration Agency in Indonesia (2016)), these areas belong to peatland. We sought a forest fire area that possessed Landsat 8 data with little cloud influence. Based on this desired condition, we selected the area around Palangkaraya, the capital of the Indonesian province of Central Kalimantan, including the Katingan and Pulang Pisau Regencies, which are located within the Central Kalimantan Province, on the island of Kalimantan (Borneo), Indonesia (Figure 1).

The spectral characteristics of the 16-multispectral AHI imager are shown in Table 1. For AVHRR, 4μm channel is suitable for detection of the hot spot (Belward et al. (1994)), and MODIS, 4μm and 11μm channels are used in the fire detection algorithm (Giglio et al. (2003)). For Landsat 8, a paper has shown that SWIR (2.1-2.3μm) is suitable for fire detection (Schroeder et al (2016).). Also for AHI, for monitoring of grassland fire in China, band 3, 4 and 7 were used (Na et al. (2018), and band 7 and band 13 are tested to detect fire in Australia (Hally et al. (2016), Wickramasinghe et al. (2016), and Liu et al. (2016)). Therefore, to investigate the AHI ability of forest fire detection, we first visually deciphered the images in each band and determined that the SWIR band (corresponding to band 6 of AHI), which

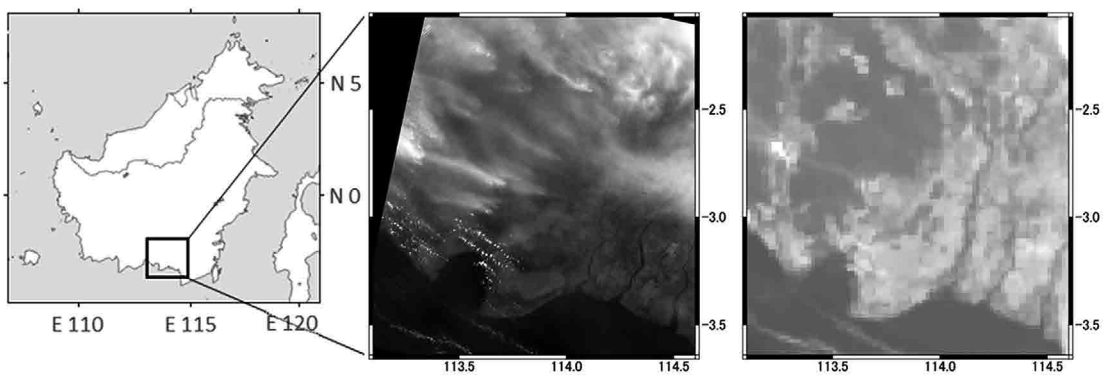

a) b) c)

Figure 1. Target area

a) The location of study area on the island of Kalimantan
b) Landsat 8 image (2015/10/22, RGB=band 6, 5, and 4), we selected fire area and other 2 land cover classes (forest area and cultivated area).
c) AHI image (2015/10/22, RGB=band 7, 6, and 5), corresponding to the Landsat data.

Table 1. Band number, horizontal resolution, and wavelength of AHI 8

Band number	1	2	3	4	5	6	7	8	9	10	11	12	13	14	15	16
horizontal resolution (km)	1	1	0.5	1	2	2	2	2	2	2	2	2	2	2	2	2
wave length (μm)	0.47	0.51	0.64	0.86	1.6	2.3	3.9	6.2	6.9	7.3	8.6	9.6	10.4	11.2	12.4	13.3

was effective in Landsat 8, was not appropriate for this study because it was more affected by smoke than the fire area. We also checked the images in bands 11 to 16, which correspond to the thermal infrared bands, and confirmed that these six images were very similar in trend. Hence we selected band 7, which is the mid-infrared band that was suitable for fire detection with low-resolution satellites, and band 13 from the thermal infrared band, that has already been used in other papers. (San-Miguel-Ayanz and Ravail (2005)). Visual interpretation from Landsat 8 band 6, 5, and 4 composite color images confirmed that fires occurred in three scenes on 2015/09/04, 2015/09/22, and 2015/10/22. Therefore, we selected the 2 AHI data sets corresponding to those shooting dates: 01/09/2015 to 25/09/2015 and 19/10/2015 to 26/10/2015.

2.2 Choose a band to detect fire time-series change

We checked whether band 7 or band 13 of the AHI is more suitable to represent the time-series change of the fire scene. The data used was from October. Since we knew from Google Earth Pro that most of the fires were caused by the spread of firebreaks associated with agricultural land development and that the target area was forested before the fire, we examined the two bands to see if we could separate the forest from the fire area. Therefore, the first question is how large fire in the forest can be detected, and the second question is that the extent of the fire can be traced along with the time series and whether the cultivated land and the fire area can be separated after the fire ends.

The first step was to see how small a fire area could be detected in either band. The Landsat 8 image of 22/10/2015 was used to decipher the fire area. Schroeder et al. (2016) state that SWIR is considered to be suitable for fire area estimation. Therefore, we used both the color composite images of bands 7, 5, and 4 in addition to band 10 of Landsat 8 to read the fire area, and set the threshold value of band 10 for visual reading when both images overlapped (Figure 2). The threshold value was set to 302.5 degrees. The range of values above this threshold was defined as the fire area in Landsat 8. In the same way, Landsat 8 was used to select the area of forest and fire site. The selected area was checked by Google Earth Pro and the pixels were selected from the areas that could be judged as uniform forest as possible.

Then, from the AHI data taken at the same time as Landsat 8, the band 7 and band 13 AHI pixels corresponding to the area containing the fire area were identified. However, since there was a discrepancy between the Landsat 8 data and the AHI data, it was necessary to visually adjust the positions. Also, since the resolution of the AHI data is 2 km, the pixels indicating the fire area include the surrounding areas that have not yet been burned or

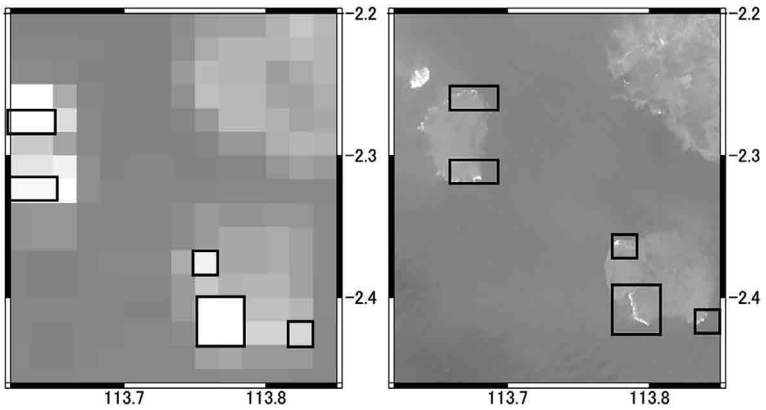

Figure 2. Example of fire area in AHI band 7 (left) and Landsat band 7, 5, 4 color image (right), 2015/10/22.

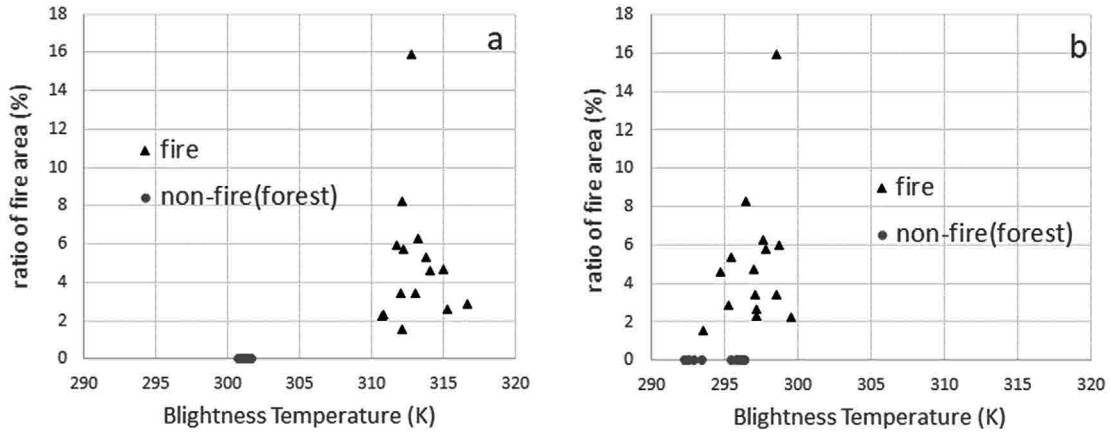

a : band 7　　b : band 13

Figure 3. Scatter diagram of AHI brightness temperature and ratio of fire area by Landsat 8. According to a), fire can be detected if the ratio of the fire in pixel is about 2% by using band 7, on the other hand, from b) we found that fire can't be detected the fire pixel even if the ratio of the fire area is over 5% by using band 13.

damaged by fire. We then examined the relationship between the percentage of fire area in the AHI and the value of the AHI. At this time, we selected the forest as the location with zero fire ratio area and calculated the AHI values for the forest before the fire to see if the pre-and-fire areas could be separated (Figure 3).

Next, we checked how fire areas could be captured in the time-series data. After the fire is extinguished, the land is used as cultivated land. Therefore, to know when the fire is extinguished, the fire area and cultivated land must be separated before the fire is extinguished. Therefore we graphed the 7-day time series of pixel changes in the AHI for the fire area, forest, and cultivated land, respectively, to see if the time-series changes in fire area could be distinguished from the time-series changes in forest and cultivated land (Figure 4). At this time, the cultivated land was deciphered from Landsat 8 and Google Earth Pro. However, since it was not possible to separate old burned areas from cultivated areas, the cultivated area pixel in the AHI includes both old burned areas and cultivated areas.

These two results were then used to determine which band was best suited to track the time-series change in fire (Figure 4).

2.3 Establishing two indices for fire analysis

By the three tracing graphs of the suitable band, we found that the graph of fire area experienced short-term fluctuations, moving up and down about every 10 minutes. In contrast, the graphs of forest area and cultivated area fluctuated smoothly in the one-day cycle. Thus, we consider that not only the high value of a suitable band but also short-term fluctuations are characteristics of fire.

To confirm this assumption, we separated the value of the band into 2 components : mean value and amplitude range of short-term fluctuations. We used the moving average method and defined it as shown in Equation (1) and (2) ;

$$\mu_{tm} = \mu(tm) = \text{mean}\ (X_t),\ (\text{unit : K}) \quad (1)$$

$$D_{tm} = D(tm) = \text{abs}\ (X_{tm} - \mu_{tm})\ (\text{unit : K}) \quad (2)$$

X_t = brightness temperature of AHI band at time t, (unit : K)

t = tm-30 ~ tm+30), (unit : minutes)

tm = time variable (unit : 10 minutes)

From time-series data, we knew that short-term fluctuations occur approximately 3 to 5 times in 2

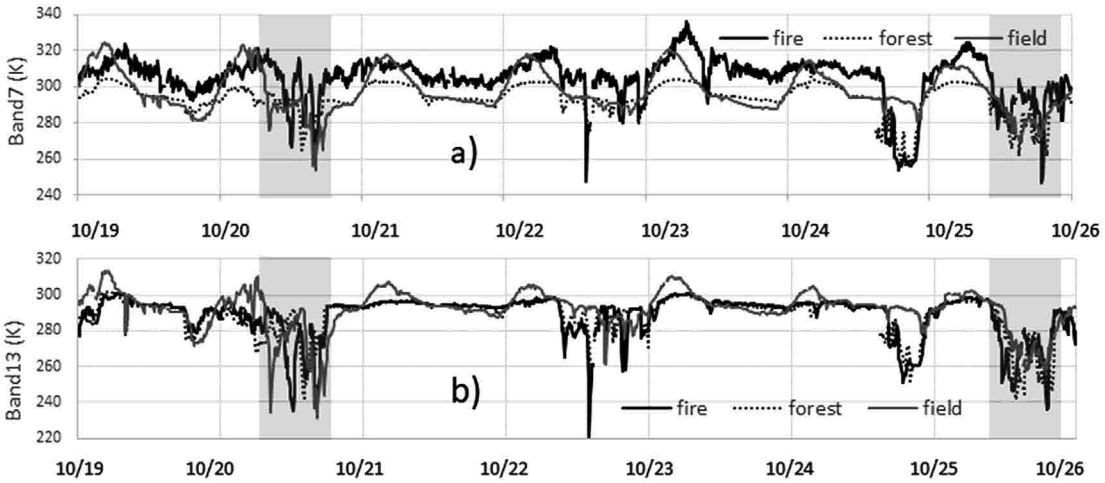

Figure 4. Graphs that follows the time series changes of 3 type area between 7 days.
Black line : fire area, dot line : forest area, gray line : cultivated area (contain old burnt area)
a : band 7, b : band 13
gray background area : Periods considered to be under the influence of clouds
From a), we can separate the fire line from forest line (because of high value) and cultivated line (because of short-term fluctuations), on the other hand, from b), we can't separate the forest area and fire area.

hours. Then we set that the time-averaged range is 1 hour, as short as possible, and including at least 1 cycle of fluctuations, every 30 minutes before and after the target time. As a longer period is set for the time-average method, it takes a longer time to calculate 2 indices and the temporal resolution of AHI could not be exploited.

We confirmed the behavior of these two indices, μ_{tm}, mean of X_t and D_{tm}, range of short-term fluctuations in X_t by applying this method to the pixels of the fire area from the October data.

We then used these two indices on time-series data from different time periods to examine the behavior of pixel values corresponding to extinguished areas and fire areas to see if these two indices are effective in tracking changes in the fire time series. To identify fire areas, we used two Landsat 8 images taken within 16 days (09/04/2015 and 09/22/2015) to visually decipher fire areas and tracked the values of AHI pixels corresponding to these areas from 01/09/2015 to 25/09/2015 (Figure 5). The unburned forest pixels were also selected to be treated as background data. The duration of the AHI data was set to be a few days longer before and after the two Landsat 8 image capture agencies to study the fire locations in the Landsat image before and after the fire.

However, due to the large scale of the fire, the cloud and smoke effects extended to the surrounding forest area, and the overall D_{tm} values were higher than the same area in October, as a result, it was difficult to decipher when the fire started. Therefore, the following index was developed based on the expectation that D_{tm} would continue to be high in the fire area.

Hence, we defined the new index, Ci. The definition of Ci is as shown in Equation (3)-(4) :

$$\begin{aligned} Tr\_i(tm) &= 1 ;\ \text{If } D_{tm} \geq i \\ &= 0 ;\ \text{If } D_{tm} < i \end{aligned} \quad (3)$$

$$Ci = \Sigma Tr\_i(t) \quad (4)$$

$$t = tm-30 \sim tm+30 \quad \text{(unit : minutes)}$$

In Equation (3), i is the threshold of D_{tm}, bigger than the D_{tm} of the unburnt area and less than that of the fire area. We tested i=3, 5, and 10, then defined i=5 as suitable to find the fire period and Ci as C5. C5 means that D_{tm} takes a value bigger than 5 C5 times within the period between tm-30 minutes

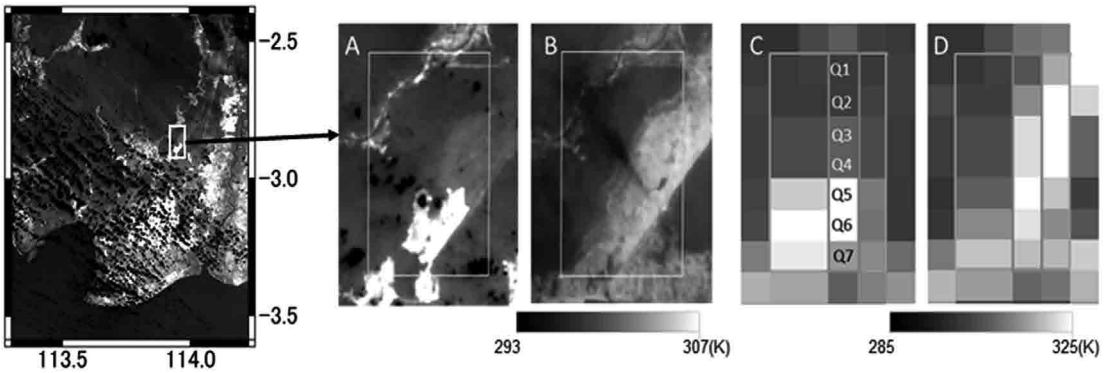

Figure 5. Area that fire spread and extinguished in 16 days. A and B are Landsat 8 band 10 image and C and D are AHI band 7 image. Date of A and C is 2005/09/04 and date of B and D is 2015/09/20.
From A and B images, we found fire area (Bright white area in imageA) expanded diagonally upward from the lower left and was extinguished within 16 days (light gray area in imageB). So we selected pixels at location (Q1 to Q7 in image C). For these pixels we calculated μ_{tm} and Ci and followed the change of these indices with the change in fire.

to tm+30 minutes, and takes an integer value from 0 to 7.

We then investigated the behavior of the pixel value corresponding to fire extinguishment and fire outbreak areas using C5 and μ_{tm}.

3. Results

3.1 Suitable band to detect fire time-series change

We estimated the ratio of fire area from between band 10 of Landsat 8 and AHI band 7 and 13 values (Figure 3) As a result, there is no relationship between the fire area ratio and the value of band 7, but the fire area is clearly separated from the forest. On the other hand, for band 13, there is a proportional relationship between the fire area percentage, but the fire area cannot be separated from the forest, then we found that band 7 is more suitable than band 13 to detect the small fire area. The percentage of fire area within a pixel required to detect band 7 was estimated from the 16 samples used in the graph. Of the area proportions within the samples used, the three from the smallest were 1.54%, the three from the smallest were 2.3%, and the three from the smallest were 2.6%. Therefore, if the fire percentage within one pixel is more than 2%, it is considered to be detectable in band 7.

And from graphs of time series change (Figure 4), we found the following ; except the period of cloud influence (10/21 and 10/25 in graph 5.), band 7 values in the fire area were always kept the value more than 10K higher than those in the forest area. On the other hand, band 13 values in both the fire area and the forest area were almost the same, therefore we decided band 7 is also more suitable than band 13 to trace the fire area. However, it was found that even in band 7, the value of cultivated land was higher than the value of fire land for a period of time during the day, so it was not possible to simply separate fire land from cultivated land using the threshold value.

3.2 Temporal characteristics of the indices

As mentioned in 3.1, the value of band 7 is not appropriate to indicate the timing of fire extinguishment as it is. Therefore, we considered using the short-term fluctuations of the pixels corresponding to the fire area as another indicator of the extent of the fire. So we calculated D_{tm} and μ_{tm} for band 7 of the AHI in October to confirm the behavior of the two indices. We selected two fire area pixels and 1 forest area pixel, traced the value of the band 7 pixels for 7 days, and calculated μ_{tm}, D_{tm}, and the calibration error of the AHI sensor, which used a value for radiometric calibration accuracy of 0.42% (AHI performance test results) Then, we compared

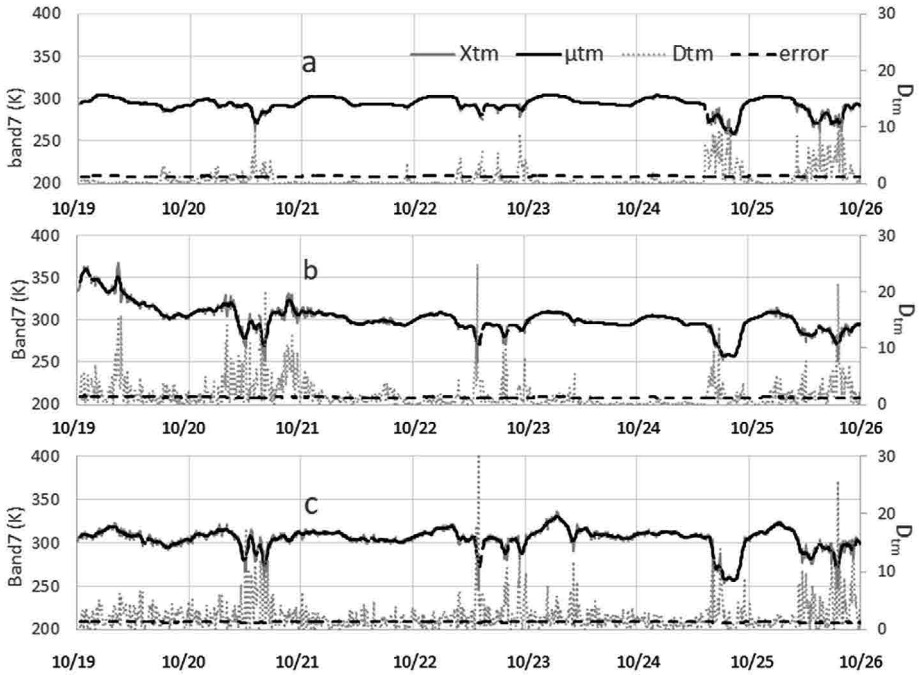

Figure 6. Comparison between forest area and fire areas by using X_{tm}, μ_{tm} and D_{tm}
a : forest area b and c : fire area

D_{tm} of forest is almost always smaller than that of fire area, b and c.
From 10/19 to 10/22, μ_{tm} of b) is higher than that of c). After 10/22, in b), both of D_{tm} and μ_{tm} are decreased and approaching the value of 2 indices of forest, but in c), D_{tm} are continued to keep the big value. And compared D_{tm} of forest and calibration error, D_{tm} of fire area > error.

the values of the fire and forest areas (Figure 6).

Next, we used μ_{tm} and C5, instead of D_{tm}, to trace the pixel that corresponded to fire breakout and spread areas. We used the dataset obtained from September and selected the area.

We traced and graphed μ_{tm} and C5 for 7 pixels (Q1 -Q7 in Figure 3). To compare it with the non-fire area, we also used the μ_{tm} of forest area (Figure 7).

From the graphs of μ_{tm} and C5 (Figure 7), we found that both μ_{tm} and C5 changed with the change in the fire area. C5 took the big value in the 1st day in Q5 to Q7, but on the 2nd day, both of C5 and μ_{tm} were decreased to the level of forest in Q7 and C5 appeared in Q3 to Q4. The C5 continued to take the value from the 1st day to the 6th day, then decreased from the 5th day to the 9th day in Q6. In Q5, C5 continued to appear from 1 day to 9th day, while increased from Q2 to Q4, continuing to take the large value until the 9th day. In addition, in these periods, μ_{tm} continued to possess a higher value than that of forest area. Hence, we assume that in these periods, the fire spread from Q7 to Q5 on the 1st to the 5th day, and from Q5 to Q2 on the 6th to 9th day. μ_{tm} got the highest value on the 8th day in Q2 to Q5 and the influence of the fire appeared in Q1, Q6, and Q7, but it was not so strong.

In contrast, in the daytime between the 10th and 12th days, μ_{tm} of Q2 to Q7 pixels were higher than that of forest area, but C5 took the value of 0 and 1 in the same period. From band 7 graphs of Figure 5, we could determine that the behavior is similar to the graph of cultivated area. Hence, we can conclude that the fire ended once in these areas. Fire restarted on the 13th day in Q7, and the influence of clouds continued in Q1 to Q7 on the 14th to the 17th day, but after the 17th day, μ_{tm} was higher than that of forest area, while C5 was 0 or 1. Only in Q1, the difference of μ_{tm} in Q1 and that of forest area was

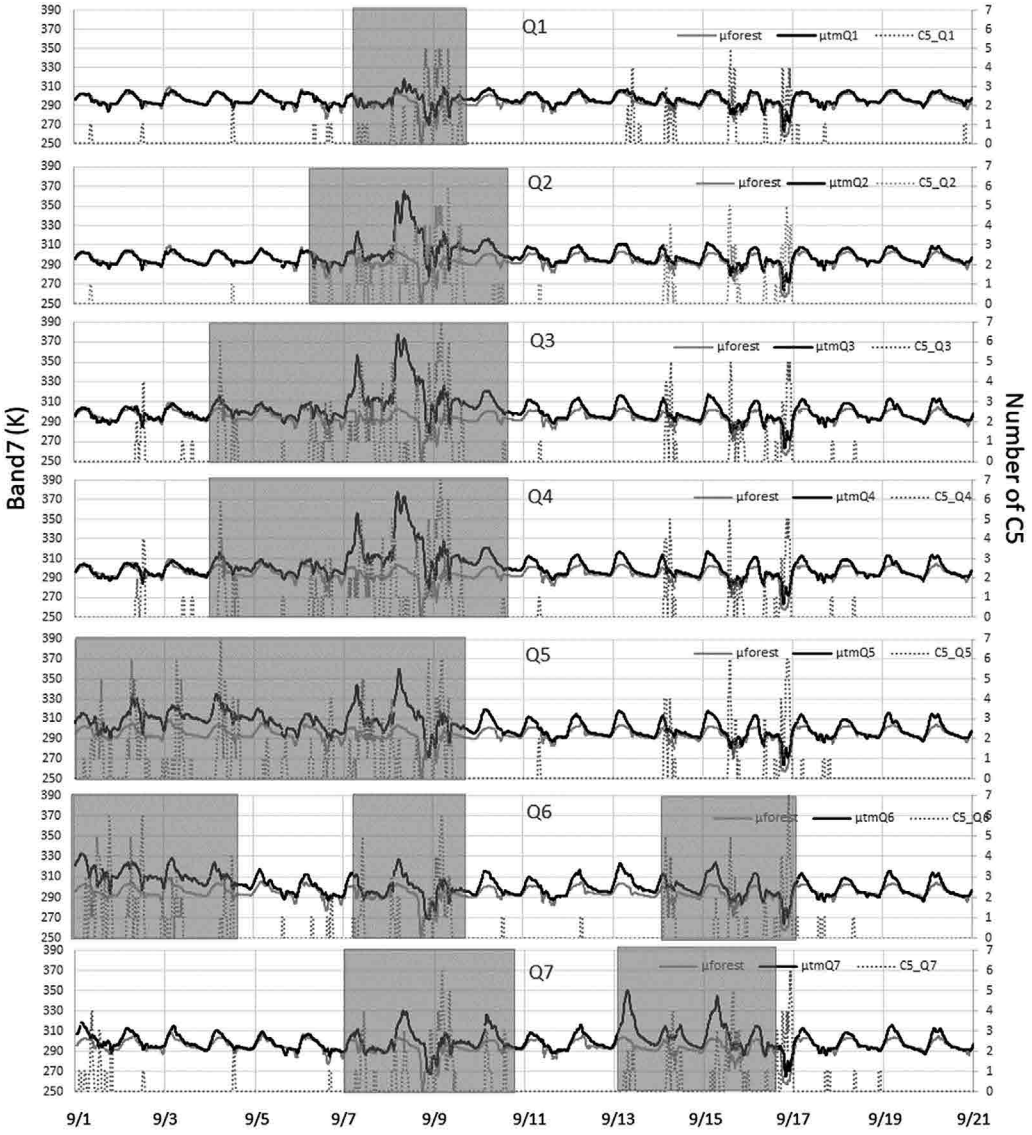

Figure 7. Trace line of 7 pixels (Q1–Q7 in Figure 2), from 2015/09/1 to 2015/09/21.
Black line : μ_{tm} of each target pixel. Gray line : μ_{tm} of forest area pixel (for references). Dot line : C5 of each target pixel. Light gray background color range : The range that was estimated that the fire was progressing using μ_{tm} and C5. Q5 and Q6 were under the effect of fire from 9/1 to 9/5. From 9/5, fire in Q6 was being extinguished, in other hand, from Q5 to Q2, the fire started to strengthen from 9/5 and became largest on 9/8. In all pixels, fire was being extinguished in 9/10. From 9/13 to 9/17, the fire started and continued in Q7, and there was the effect in Q1 to Q6.

small, except for the 8th to 10th day. Therefore, we can assume that the influence of fire was small in Q1.

4 . Discussion

4.1 Indices and fire area

Comparing the time series of the graphs for the fire and non-fire regions (Fig. 5), it was found that

the graph for the fire region in band 7 shows a short-term variation with a width distinguishable from the other two graphs. From graph 6, the amplitude of the values was deciphered to be about 5 in the fire region. Therefore, even in the graph showing the relationship between the values of band 7 and the area of the fire area, it can be assumed that each pixel has a shift of about ±5 respectively concerning the original temperature of the fire area. This misalignment may be one of the reasons why we cannot find a relationship between the fire area and band 7.

From the graph in Fig. 6, it is confirmed that the D_{tm} of forest area (a) is small enough compared to the calibration error, except for 10/20 and 10/24-25. On the other hand, in (b) and (c), it was found that D_{tm} tended to take a large value (more than 5) when the value of μ_{tm} continuously took more than 300k. The fact that the value of D_{tm} is larger in the fire area and that the value of D_{tm} for the forest is larger in the September time series data than in the October time series data suggests that one of the causes of this short-term oscillation is the effect of smoke in the fire area. Although it is difficult to separate smoke and clouds at a distance from the fire source, since smoke is hotter than clouds, it is considered to be a fire when μ_{tm} increases with D_{tm} and a cloud when μ_{tm} decreases.

4.2 Characteristics of the indices

At the stage of the fire, μ_{tm} and D_{tm} (or Ci) increase almost simultaneously, but later, even after D_{tm} and Ci decrease, μ_{tm} remains about 10 degrees higher than that of the forest during the daytime, indicating a transition to a state similar to the graph of temperature change in the cultivated land after the fire. Therefore, it is inappropriate to use μ to estimate the fire suppression time, and it is necessary to use D_{tm} (Ci).

So, what are the possible causes of D_{tm}? According to the experiment of USUP et al. (2004), when a peat fire occurs, the drying of the peat layer occurs first. When the temperature of the dry peat rises to 260°C, pyrolysis and oxidation of peat occur, and when the temperature rises above 260°C, pyrolysis and oxidation of char occur. As a result, the peatland fire is progressing with the temperature fluctuating from 250°C to 370°C, which may be regarded as a relatively short-term temperature fluctuation in the range of 2 km resolution. In this case, D_{tm} in the fire area is always considered to be larger than the value of D_{tm} in the non-fire area.

However, in the D_{tm} graph of the forest area shown in Fig. 6a, we can see that the D_{tm} value increases and the μ_{tm} value decreases from October 24 to 25. Since the range of variation of D_{tm} during this period is the same in the forest area and the fire area, it is considered that the range of variation of D_{tm} is the same in the fire area and the forest area, and therefore, the variation of D_{tm} value does not include the temperature change peculiar to the fire area, and the influence of clouds and smoke is more significant.

Na et al. (2018), the target area of the fire in the Mongolian steppe, also estimated the occurrence of the fire from the brightness temperature of band 7, but the burned area was detected in band 4, and the direction of the fire was estimated from its expansion. Since it took two days and eight hours from the start of the fire to the end of the fire, it is thought that the change in the burned area was sufficiently captured even at 2 km resolution. On the other hand, in the peatland, the target area of this study, the fire temperature is relatively low and the effect of smoke is large. The fire in each pixel lasts for a week or more at most, and the smoke effect also continues. Therefore, it was not possible to estimate the burned area in Band 4.

In the case of a typical forest fire, the temperature is estimated to be about 800°C. In this case, the difference in brightness temperature between the fire area and the burned area is likely to be larger than that between the fire area and the burned area in peatland. In this case, the difference in brightness temperature between the fire area and the burned area is likely to be larger than the difference

between the fire area and the burned area in a peatland. Therefore, it is highly likely that the brightness temperature of the bands can separate these two.

Conversely, the indices of D_{tm} and Ci are likely to be effective in long-term, smoke-intensive areas such as peatland fires, but D_{tm} may not be effective in other cases, and its threshold may change.

5. Conclusions

In this study, we found that band 7 of HIMAWARI 8/AHI could follow in 10-minutes steps from the early stage of fire to extinction. Also, we found that not only the value of band 7 itself but also the short-range fluctuation (20-40 minutes for 1 cycle) of value is the feature of the fire pixel. Then we decided on two indices, μ_{tm}, 1-hour time average value of band 7 and D_{tm}, range of short-term fluctuation that was able to be detected using the high-temporal resolution satellite data. The μ_{tm} of the fire pixel value is always higher than that of the forest area pixel, then the fire area is distinguishable from the forest area only by μ_{tm}. On the other hand, sometimes, D_{tm} decrease although μ_{tm} continuous to be high, and we can estimate that fire become to extinguish. And using these two indices, we could assume the fire intensity of the target fire area and the period from fire occurrence to extinguishment. However, even if the value of D_{tm} is large, if μ_{tm} is low, it is considered to be the effect of clouds. So, it can not be judged as a fire, simply because the value of D_{tm} is large. By combining the two indices, it was possible to observe the fire spreading over 10 km in about 10 days.

In this study, we confirmed how a fire is shown from AHI data, and in the next step, we want to analyze the AHI data with ground truth data, for example, the direction of wind and condition of burnt area (e.g., the fire is not so strong that only tree crowns were burnt, or the fire is so strong that tree trunks were carbonized), and burnt biomass itself. We think there are still some uncertainties in the factors of Dtm and Ci. Therefore, we want to confirm how these indices are related to specific processes, for example, the relationship between two indices and burnt biomass. It is considered that there is a relationship between D_{tm} and smoke, which is one of the causes of air pollution. Then we would like to investigate if there is a quantitative relationship between these indices from satellite data and burnt biomass.

Acknowledgements

We would like to thank the all reviewers for providing important comments.

（受付日2020.4.23，受理日2022.4.11）

References

1. Meteorological Satellite Center of JMA, AHI-8 performance results by ground test, https://www.data.jma.go.jp/mscweb/ja/himawari89/space_segment/doc/AHI8_performance_test_jp.pdf.
2. Antonovsky, M.Y., Ter-Mikhaelian, M.T., Furyaev, V.V., 1989. A Spatial Model of Long-Term Forest Fire Dynamics and Its Application to Forests in Western Siberia. IIASA Working Paper. IIASA, Laxenburg, Austria : WP-89-109.
3. Badan Restorasi Gambut (BRG) in Indonesia, 2016, Peta Indikatif Prioritas Restorasi Provinsi Karimantan Tengah, 2016. https://brg.go.id/wp-content/uploads/2017/03/BRG_Peta-Restorasi-Kalteng.pdf
4. Belward, A.S., Kennedy, P.J., Grégoire, J.M, 1994, The limitations and potential of AVHRR GAC data for continental scale fire studies. International Journal of Remote Sensing, 15(11), pp. 2215-2234.
5. Bessho, K., Date, K., Hayashi, M., Ikeda, A., Imai, T., Inoue, H., Kumagai, Y., Miyakawa, T., Murata, H., Ohno, T., Okuyama, A., Oyama, R., Sasaki, Y., Shimazu, Y., Shimoji, K., Sumida, Y., Suzuki, M., Taniguchi, H., Tsuchiyama, H., Uesawa, D., Yokota, H., Yoshida, R., 2016. An Introduction to Himawari-8/9－Japan's New-Genera-

tion Geostationary Meteorological Satellites. Journal of the Meteorological Society of Japan, 94(2), pp.151-183.

6. Böhme, C., Bouwer, P., Prinsloo, M.J., 2015. Real-Time Stream Processing for Active Fire Monitoring on Landsat 8 Direct Reception Data. 2015. The International Archives of the Photogrammetry, Remote Sensing and Spatial Information Sciences, Volume XL-7/W3, pp.765-770.

7. Boles, S.H. and Verbyla, D.L., 1999. Effect of scan angle on AVHRR fire detection accuracy in interior Alaska. International Journal of Remote Sensing 20(17), pp.3437-3443.

8. Bonan, G.B., and Shugart, H.H., 1989. Environmental Factors and Ecological Processes in Boreal Forests. Annual Review of Ecology and Systematics, 20, pp.1-28.

9. Cahoon, Jr., D.R., Stocks, B.J., Levine, J.S., Cofer III, W.R., Pierson, J.M., 1994. Satellite analysis of the severe 1987 forest fires in northern China and southeastern Siberia. Journal of Geophysical Research, 99(9), pp.18627-18638.

10. Calle, A., Casanova, J.L., Romo A., 2006. Fire detection and monitoring using MSG Spinning Enhanced Visible and Infrared Imager (SEVIRI) data. Journal of Geophysical Research, 111, G04S06.

11. Cary, G.J., Keane, R.E., Gardner, R.H., Lavorel, S., Flannigan, M.D., Davies, I.D., Li, C., Lenihan, J. M., Rupp, T.S., Mouillot, F., 2006. Comparison of the sensitivity of landscape-fire-succession models to variation in terrain, fuel pattern, climate and weather. Landscape Ecology, 21(1), pp. 121-137.

12. Fatkhuroyan, Wati, T., Panjaitan, A., 2017. Forest fires detection in Indonesia using satellite Himawari-8 (case study : Sumatera and Kalimantan on august-october 2015). IOP Conference Series : Earth and Environmental Science, 54(1).

13. Freeborn, P.H., Cochrane, M.A., Wooster, M.J., 2014. A Decade Long, Multi-Scale Map Comparison of Fire Regime Parameters Derived from Three Publically Available Satellite-Based Fire Products : A Case Study in the Central African Republic. Remote Sensing. 6(5), pp.4061-4089.

14. Fuchs, E.M., Stein, E., Strunz, G., Strobl, C., Frey, C., 2015. Fire Monitoring—The Use of Medium Resolution Satellites (AVHRR, MODIS, TET) for Long Time Series Processing and the Implementation in User Driven Applications and Services. 2015, The International Archives of the Photogrammetry, Remote Sensing and Spatial Information Sciences, Volume XL-7/W3, pp.797-804.

15. Giglio, L., Kendall, J., Justice, C.O., 1999. Evaluation of global fire detection algorithms using simulated AVHRR infrared data. International Journal of Remote Sensing 20(10), pp.1947-1985.

16. Giglio, L., Descloitres, J., Justice, C.O., Kaufman, Y.J., 2003. An Enhanced Contextual Fire Detection Algorithm for MODIS. Remote Sensing of Environment 87(2-3), pp.273-282.

17. Giglio, L., Schroeder, W., Justice, C.O., 2016. The collection 6 MODIS active fire detection algorithm and fire products. Remote Sensing of Environment, 178, pp.31-41.

18. Hally, B., Wallace, L., Reinke, K., Jones, S., 2016. Assessment of the Utility of the Advanced Himawari Imager to Detect Active Fire over Australia. International Archives of the Photogrammetry, Remote Sensing and Spatial Information Sciences, XLI-B8, pp.65-71.

19. Hawbaker, T.J., Radeloff, V.C., Syphard, A.D., Zhu, Z., Stewart, S.I., 2008. Detection rates of the MODIS active fire product in the United States. Remote Sensing of Environment, 112, pp.2656-2664.

20. Huang, X and Rein G., 2019, Upward-and-downward spread of smoldering peat fire., Proceedings of the Combustion Institute 37, pp.4025-4033.

21. IPCC AR5, Climate Change 2014 : Impacts, Adaptation, and Vulnerability, Summary for Policymakers-IPCC Working Group II, from http://ipcc-wg2.gov/AR5/images/uploads/

WG2AR5_SPM_FINAL.pdf.

22. Jang, E., Kang, Y., Jungho, Im, J., Lee, D.W., Yoon, J., Kim, S.K., 2019. Detection and Monitoring of Forest Fires Using Himawari-8 Geostationary Satellite Data in South Korea. Remote Sensing 11(3), 271.

23. Jolly, W.M., Cochrane, M.A., Freeborn, P.H., Holden, Z.A., Brown, T.J., Williamson, G.J., Bowman, D.M.J.S., 2015. Climate-induced variations in global wildfire danger from 1979 to 2013. Nature Communications 6, Article number : 7537, published July 14, 2015, from http://www.nature.com/articles/ncomms8537

24. Keane, R.E., Cary, G.J., Ian D. Davies, I.D., Flannigan, M.D., Gardner, R.H., Lavorel, S., Lenihan, J.M., Li, C., Ruppi, T.S., 2004. A classification of landscape fire succession models : spatial simulations of fire and vegetation dynamics. Ecological Modelling, 179(1), pp.3-27.

25. Lecomte, N., Simard, M., Bergeron, Y., Larouche, A., Asnong, H., Richard, P.J.H., 2006. Effects of fire severity and initial tree composition on understorey vegetation dynamics in a boreal landscape inferred from chronosequence and paleoecological data. Journal of Vegetation Science, 16(6), pp.665-674.

26. Li, C., Ter-Mikaelian, M.T., Perera, A.H., 1995. Modelling interactions between fire regime and forest landscape. Proceedings of the 9th International Geomatics Conference. Geomatics Canada, Ottawa, pp.1-7.

27. Liu, X., He, B., Quan, X., Yebra, M., Qiu, S., Yin, C., Liao, Z., Zhang, H., 2018. Near Real-Time Extracting Wildfire Spread Rate from Himawari-8 Satellite Data. Remote Sensing 10(10), 1654.

28. Liu, Y., Goodrick, S.L. Stanturf, J.A., 2013. Future U.S. wildfire potential trends projected using a dynamically downscaled climate change scenario. Forest Ecology and Management, 294(15), pp.120-135.

29. Morisette, J.T., Giglio, L., Csiszar, I., Setzer, A., Schroeder, W., Morton, D., Justice, C.O., 2005. Validation of MODIS Active Fire Detection Products Derived from Two Algorithms. Earth Interactions, 9, pp.1-24.

30. Na, L., Zhang, J., Bao, Y., Bao, Y., Na R., Tong, S., Si, A., 2018. Himawari-8 Satellite Based Dynamic Monitoring of Grassland Fire in China-Mongolia Border Regions. Sensors 2018, 18(1), 276.

31. Page, S.E., Siegert, F., O Rieley, J, Boehm, H.D. V, Jaya, A., Limin, S., 2002, The amount of carbon released from peat and forest fires in Indonesia during 1997, Nature 420, pp.61-65.

32. Rauste, Y., Herland, E., Frelander, H., Soini, K., Kuoremaki, T., Roukari, A., 1997. Satellite-based forest fire detection for fire control in boreal forests. International Journal of Remote Sensing, 18(12), pp.2641-2656.

33. San-Miguel-Ayanz, J. and Ravail, N., 2005. Active Fire Detection for Fire Emergency Management : Potential and Limitations for the Operational Use of Remote Sensing. Natural Hazards 35, pp.361-376.

34. Schroeder, W., Prins, E., Giglio, L., Csiszar, I., Schmidt, C., Morisette J., Morton, D., 2008. Validation of GOES and MODIS active fire detection products using ASTER and ETM+ data. Remote Sensing of Environment, 112, pp.2711-2726.

35. Schroeder, W., Csiszar, I., Giglio, L., Schmidt, C., 2010. On the use of fire radiative power, area, and temperature estimates to characterize biomass burning via moderate to coarse spatial resolution remote sensing data in the Brazilian Amazon. Journal of Geophysical Research, 115, D21I21.

36. Schroeder, W., Oliva, P., Giglio, L., Quayle, B., Lorenz, E., & Morelli, F., 2016. Active fire detection using Landsat-8/OLI data. Remote Sensing of Environment. 185, pp.210-220.

37. Seielstad, C.A., Riddering, J.P., Brown, S.R., Queen, L.P., & Hao, W.M, 2002. Testing the sensitivity of a MODIS-like daytime active fire detection model in Alaska using NOAA/AVHRR infrared data. Photogrammetric Engineering &

Remote Sensing 68, pp.831-838.
38. Wickramasinghe, C.H., Jones, S., Reinke, K., Wallace, L., 2016. Development of a Multi-Spatial Resolution Approach to the Surveillance of Active Fire Lines Using Himawari-8. Remote Sensing. 8(11), 932.
39. Wiggins, E.B, Czimczik, C.I., Santos, G.M., Chen, Y., Xu, X., Holden, S.R., Randerson, J.T., Harvey, C.F., Kai, F.M., Yu, L.E., 2018, Smoke radiocarbon measurements from Indonesian fires provide evidence for burning of millennia-aged peat. Proceedings of the National Academy of Sciences of the United States of America, 115(49), pp.12419-12424.
40. Wooster, M.J., Roberts, G., and Perry, L.W., 2005, Retrieval of biomass combustion rates and totals from fire radiative power observations : FRP derivation and calibration relationships between biomass consumption and fire radiative energy release. Journal of geophysical Research, 110, D24311.
41. Xie, Z., Song, W., Ba, R., Li, X., Xia, L., 2018. A Spatiotemporal Contextual Model for Forest Fire Detection Using Himawari-8 Satellite Data. Remote Sensing. 10(12), 1992.
42. Xu, W., Wooster, M.J., Roberts, G., Freeborn, P., 2010. New GOES imager algorithms for cloud and active fire detection and fire radiative power assessment across North, South and Central America. Remote Sensing of Environment. 114, pp.1876-1895.
43. Xu, W., Wooster, M.J., Kaneko, T., He, J., Zhang, T., Fisher, D., 2017. Major advances in geostationary fire radiative power (FRP) retrieval over Asia and Australia stemming from use of Himarawi-8 AHI. Remote Sensing of Environment. 193, pp.138-149.
44. Yang, J., He, H.S., Sturtevant, B.R., Miranda, B.R., & Gustafson, E.J., 2008. Comparing effects of fire modeling methods on simulated fire patterns and succession : a case study in the Missouri Ozarks. Canadian Journal of Forest Research, 38, pp.1290-1302.